Climate Variability in the Equatorial Pacific Ocean Induced by Decadal Variability of Mixing Coefficient

CHUAN JIANG HUANG* AND WEI WANG

Physical Oceanography Laboratory, Ocean University of China, Qingdao, China

RUI XIN HUANG

Department of Physical Oceanography, Woods Hole Oceanographic Institution, Woods Hole, Massachusetts

(Manuscript received 4 April 2005, in final form 1 September 2006)

ABSTRACT

The circulation in the equatorial Pacific Ocean is studied in a series of numerical experiments based on an isopycnal coordinate model. The model is subject to monthly mean climatology of wind stress and surface thermohaline forcing. In response to decadal variability in the diapycnal mixing coefficient, sea surface temperature and other properties of the circulation system oscillate periodically. The strongest sea surface temperature anomaly appears in the geographic location of Niño-3 region with the amplitude on the order of 0.5°C, if the model is subject to a 30-yr sinusoidal oscillation in diapycnal mixing coefficient that varies between 0.03×10^{-4} and 0.27×10^{-4} m^2 s^{-1}. Changes in diapycnal mixing coefficient of this amplitude are within the bulk range consistent with the external mechanical energy input in the global ocean, especially when considering the great changes of tropical cyclones during the past decades. Thus, time-varying diapycnal mixing associated with changes in wind energy input into the ocean may play a nonnegligible role in decadal climate variability in the equatorial circulation and climate.

1. Introduction

Theory of oceanic general circulation and climate change has gradually evolved over the past decades. It is well known that oceanic general circulation models are sensitively dependent on parameterizations of subgrid-scale processes. In particular, models are very sensitive to the parameterization of diapycnal mixing. Different schemes of diapycnal mixing have been postulated and tested extensively, including the common practice of using time-invariant diapycnal mixing coefficient specified a priori.

A new paradigm of theory of the oceanic general circulation that emphasizes the critical role of external mechanical energy in maintaining the oceanic general circulation has recently been developed. Because diapycnal mixing in the oceanic interior raises the center of mass, external mechanical energy is required to sustain diapycnal mixing in the subsurface layers (Munk and Wunsch 1998; Wunsch and Ferrari 2004; Huang 1999, 2004).

Although the ocean receives a huge amount of thermal energy from solar radiation, it cannot convert the thermal energy into mechanical energy efficiently. The inability of the ocean to convert thermal energy through the air–sea interface is due to the peculiar fact that the ocean is heated and cooled from the upper surface only (Sandström 1908, 1916; Huang 1999; Wang and Huang 2005). (The contribution from geothermal heating is negligible.) As a moving system, thus, the ocean requires external sources of mechanical energy to overcome friction. The primary sources of mechanical energy for the ocean include tidal dissipation and wind energy input through the upper surface (Munk and Wunsch 1998).

Although tides have been omitted in oceanic general circulation for many decades, it is now commonly acknowledged that tidal dissipation is one of the primary

* Current affiliation: The First Institute of Oceanography, State Oceanic Administration, Qingdao, China.

Corresponding author address: Wei Wang, Physical Oceanography Laboratory, Ocean University of China, Qingdao 266003, Shandong, China.
E-mail: wei@ouc.edu.cn

DOI: 10.1175/JPO3060.1

energy sources that support diapycnal mixing in the oceanic interior, especially in the deep ocean. It is estimated that the total tidal dissipation rate in the open ocean is on the order of 0.7–0.9 TW, which may contribute 50% of the energy required for sustaining diapycnal mixing in the subsurface ocean (Munk and Wunsch 1998).

However, energy input from wind stress may play a vitally important role in regulating climate variability through changes in diapycnal mixing. According to recent studies, wind energy input to the Ekman layer is about 3 TW (Wang and Huang 2004a; Alford 2003a) and wind energy input to the geostrophic current is about 1 TW (Wunsch 1998). Over the past 50 yr, these sources of energy varied greatly (Alford 2003a; Wang and Huang 2004a; Huang et al. 2006). In addition, wind energy input to surface waves is estimated at 60 TW (Wang and Huang 2004b). Although it is believed that most of this energy is dissipated in the upper ocean, the potential role of surface waves dissipation in regulating the thermohaline circulation remains unclear.

Tropical cyclones play an important role in driving the thermohaline circulation and thereby in regulating regional and global climate (Emanuel 2001). Because of the strong wind associated with tropical cyclones, a large amount of energy can be input to the ocean, which can substantially enhance diapycnal mixing at low latitudes. Recent studies showed that the energy dissipation rate of tropical cyclones in the western North Pacific and North Atlantic Oceans has nearly doubled over the past 30 yr (Emanuel 2005).

There may be some special long-term tidal components that can induce climate variability on decadal time scales or longer, such as potential surface temperature variability in coastal seas associated with the 18.61-yr-period tides (Loder and Garrett 1978). In general, however, tidal dissipation can be considered nearly constant over time scales shorter than centennial.

Because wind stress energy input varies greatly, the energetic level of internal waves should also change in response. An important theoretical question is whether a time-varying diapycnal mixing rate can induce noticeable climate variability. This basic idea has been tested in a three-dimensional oceanic general circulation model. Boos et al. (2004) carried out numerical experiments with a time-varying diapycnal mixing rate for an Atlantic-like model ocean. Their results indicate that transient diapycnal mixing can effectively drive the meridional overturning, as long as the mixing was not highly localized in space.

In the Pacific Ocean strong evidences have shown that there exists decadal variability in climate records with a typical period of 15–25 and 50–70 yr (Mantua and Hare 2002; Mantua et al. 1997). Previous studies of the decadal variability in the Pacific Ocean have been focused on nonlinear air–sea interaction, without taking into consideration changes in the diapycnal mixing coefficient associated with the wind stress energy input into the ocean. Some parameterizations, such as the *K*-profile parameterization scheme (Large et al. 1994), the Pacanowski and Philander (1981) scheme, and the Mellor and Yamada (1982) scheme, may partially include the effects; however, these schemes may not represent the subgrid-scale internal waves and turbulent processes accurately, and thus much room is left for further study.

In contrast to the nearly constant dissipation rate associated with tides on time scales shorter than centennial, energy input from wind stress varies greatly on time scales shorter than centennial. In the equatorial Pacific Ocean the mechanical energy sustaining diapycnal mixing comes partly from the local wind energy input and partly from wind energy input at middle/high latitudes. Most of wind energy input to the ocean is concentrated over the Antarctic Circumpolar Current region and the storm-track regions in the Northern Hemisphere, and their variability is larger than that in the equatorial ocean (Alford 2003a; Wang and Huang 2004a; Huang et al. 2006). For example, extratropical near-inertial energy input has increased by approximately 40%, but the input in the tropical regime has remained nearly constant over the past 50 years (Alford 2003a).

In the ocean, the equilibrium of energy of internal waves and turbulence is nonlocal. Since wind energy input at low latitudes is smaller than that at high latitudes, there are indications that an equatorward energy transfer is at work in the World Oceans. In fact, near-inertial energy fluxes in both hemispheres are directed overwhelmingly equatorward (Alford 2003b). Nagasawa et al. (2000) found that near-inertial waves excited at 10°–45°N in the North Pacific by midlatitude storms and tropical cyclones can propagate equatorward down to 5°–15°N, where their energy is transferred to small-scale dissipation by parametric subharmonic instability, enhancing diapycnal mixing in these areas. Moreover, wind-induced near-inertial energy may be redistributed by advective processes (Zhai et al. 2004). Some studies have revealed that wind stress variability in the Southern Ocean has a noticeable effect on the equatorial circulation. For example, strong wind stress in the Southern Ocean can enhance westward surface currents in the equatorial Pacific Ocean (McDermott 1996, Fig. 10 in his paper). Therefore, the cause of variability of diapycnal mixing in the equatorial Pacific Ocean is not limited to changes in wind

stress in the equatorial ocean; instead, it should be linked to changes in wind stress outside of the equatorial band. Some recent studies have reviewed the relationship of mechanical energy input and diapycnal mixing in the ocean (Garrett and St. Laurent 2002; Wunsch and Ferrari 2004). However, our understanding of processes sustaining internal waves and turbulence in the ocean remains rudimentary. At this stage, thus, it is helpful to explore the effect of variability in diapycnal mixing in separation from changes in local wind.

The goal of this investigation is to use a numerical model to test the response of the equatorial circulation to changes in diapycnal mixing coefficient on decadal time scales. The model is based on an isopycnal model and set for the equatorial Pacific Ocean. Diapycnal mixing coefficient is treated as a parameter independent of the local wind stress, which implies the influence of the variability of the global wind stress energy on the equatorial Pacific Ocean. The model details are discussed in section 2. Several sets of numerical experiments were carried out, and the results of these experiments are discussed in section 3. Because we do not yet know the exact pathways of energy conversion from wind energy to energy of internal waves and turbulence supporting diapycnal mixing, diapycnal mixing coefficient and its time variability are specified a priori. The conclusions are drawn in section 4.

2. Model formulation

The Hallberg Isopycnal Model based on the isopycnal coordinate (Hallberg 2000; Hallberg and Rhines 1996; Thompson et al. 2002) was used in our numerical experiments. The major advantage of using an isopycnal coordinate model is that such a model can substantially reduce the artificial diapycnal mixing associated with the vertical/horizontal advection in the z-coordinate model (Griffies et al. 2000).

The model domain covers the equatorial Pacific within 30°S–30°N and 123°E–69°W, with a modest horizontal resolution of 1° by 1°. The model has 25 layers in the vertical direction, including a Kraus and Turner (1967) bulk mixed layer and a layer underneath that acts as a buffer layer between the mixed layer and the layers below. The remaining 23 layers are of density σ_2 = 30.8, 31.8, 32.6, 33.1, 33.5, 33.9, 34.2, 34.5, 34.8, 35.1, 35.4, 35.7, 36.0, 36.2, 36.4, 36.6, 36.75, 36.85, 36.92, 36.965, 37.005, 37.04, and 37.085 kg m^{-3}. The reference pressure is set to 2.0×10^7 Pa. The Scripps topography with a horizontal resolution of 1° is used (Gates and Nelson 1975) with a maximal depth of 5500 m.

The model is initiated with the temperature and salinity conditions in January taken from the Levitus climatology (Levitus and Boyer 1994; Levitus et al. 1994). The Florida State University (FSU) monthly mean climatology of wind stress with a horizontal resolution of 2° by 2° is used (Legler and O'Brien 1988), which has been interpolated linearly to the grids in this study. The sea surface temperature (SST) and salinity (SSS) are relaxed toward the monthly mean climatology (Levitus and Boyer 1994; Levitus et al. 1994) with a relaxation time of 30 days for SST and 120 days for SSS (for a mixed layer 50 m thick). Sponge layers are placed along the northern/southern boundaries of the model basin, with eight rows of grids, and within the sponge layer both temperature and salinity are relaxed toward the Levitus monthly mean climatology with a relaxation time of 1 day at the boundary and increased to 2^n days to the nth row from the northern/southern boundaries; thus, the relaxation time is 128 days for the innermost grids of the sponge layers.

The horizontal viscosity is parameterized as $\max(0.05\Delta, 0.4\Delta^2\sqrt{D_T^2 + D_S^2})$, where Δ is the grid spacing, $D_T = u_x - v_y$, and $D_S = u_y + v_x$ (Smagorinsky 1963; Griffies and Hallberg 2000). The vertical viscosity coefficient is set to 10^{-4} m^2 s^{-1}. The isopycnal thickness diffusion coefficient is set to 500 m^2 s^{-1}, and the horizontal diffusion coefficient is set to 1000 m^2 s^{-1} (Gent and McWilliams 1990). The nonlinear equation of state by Wright (1997) is used. A time-splitting scheme is used (Hallberg 1997), with the barotropic time step of 120 s, the baroclinic time step of 3600 s, and the temperature/salinity time step of 3600 s.

3. Experimental results

The model ocean was first spun up from an initial state with a fixed diapycnal mixing coefficient (DMC hereinafter) of $\kappa_d^0 = 0.15 \times 10^{-4}$ m^2 s^{-1} for 90 yr to reach a quasi-equilibrium state. Afterward, the model was restarted from this quasi-equilibrium state and run for an additional 60 yr except in experiment F, which was run for 110 yr, under the following time-dependent formula for DMC:

$$\kappa_d = \kappa_d^0 + \Delta\kappa_d \sin[(2\pi t)/T], \quad (1)$$

where $\Delta\kappa_d$ is the amplitude of the variation (m^2 s^{-1}), t is the time (yr), and T is the period of the variation (yr). There are six categories of numerical experiments in this study, experiments A–F (Table 1). Experiment A is a standard run with $\Delta\kappa_d = 0$. Experiment B corresponds to $\Delta\kappa_d = 0.12 \times 10^{-4}$ m^2 s^{-1} with a period of 4 yr. There are four runs in experiment C, where the period of the variation of DMC is fixed at 10 yr, and the amplitude of the oscillation is selected as $\Delta\kappa_d = 0.12 \times 10^{-4}$, $\Delta\kappa_d = 0.09 \times 10^{-4}$, $\Delta\kappa_d = 0.06 \times 10^{-4}$, and $\Delta\kappa_d = 0.03 \times 10^{-4}$ m^2 s^{-1}, corresponding to experiments C, C1, C2, and C3, respectively. In experiment D,

TABLE 1. DMC used in experiments: $\kappa_d = \kappa_d^0 + \Delta\kappa_d \sin 2\pi t/T$, $\kappa_d^0 = 0.15 \times 10^{-4}$ m^2 s^{-1}, $\Delta\kappa_d$ is the amplitude of the mixing rate (10^{-4} m^2 s^{-1}), and T is the period of mixing (yr). DMC is constant in both expts A and W1. DMC is a local variable in expts D1–D12, and the regions for these experiments are shown in Fig. 1a. Wind stress has decadal variability in expts W1 and W2.

Expts	A	B, C, D, E, F	C1, C2, C3	D1–D12	W1, W2
T (yr)	—	4, 10, 30, 20, 50	10	30	—, 10
$\Delta\kappa_d$ (10^{-4} m^2 s^{-1})	—	0.12	0.09, 0.06, 0.03	0.12	—, 0.12

the period of the DMC variation is 30 yr, and the amplitude of the variation is $\Delta\kappa_d = 0.12 \times 10^{-4}$ m^2 s^{-1}. Twelve additional sets of experiments were also carried out for the cases with a 30-yr period. For experiments D1–D12, the DMC varies with time, but it is confined to specific zones (Fig. 1a). Experiment E corresponds to $\Delta\kappa_d = 0.12 \times 10^{-4}$ m^2 s^{-1} with a period of 20 yr and experiment F corresponds to $\Delta\kappa_d = 0.12 \times 10^{-4}$ m^2 s^{-1} with a period of 50 yr.

In the following discussion, experiment A will be taken as the standard run, and results from other experiments will be examined in terms of their deviations from experiment A.

a. Experiments with DMC varied over the whole model basin

The most outstanding feature induced by periodic change in DMC is the periodic change in sea surface temperature anomaly (SSTA). SSTA appears primarily in the central and eastern equatorial Pacific, in particular at the geographic location called Niño-3 (5°S–5°N and 150°–90°W). The minimal (maximal) SSTA appears at the time of DMC maximal (minimal). For experiments run under the same amplitude of variability in DMC, the amplitude of a SSTA in Niño-3 increases as the period of the DMC becomes longer (Fig. 2). Although the variations of DMC in these experiments are sinusoidal, the time series of SSTA in Niño-3 is not exactly sinusoidal. In fact, the amplitudes of SSTA in the positive phase are slightly larger than those in the negative phase. For example, for experiment B (D) with a period of 4 (30) yr, the amplitude of SSTA is −0.16°C (−0.27°C) appearing at the time of maximal DMC and 0.20°C (0.40°C) appearing at the time of minimal DMC. As a result, the mean SST averaged over the period of the cycle in Niño-3 (defined as $\overline{\text{SST}} = (1/T)\int_0^T \text{SST}\, dt$, where T is the period of oscillation in DMC) is slightly different than the climatological mean

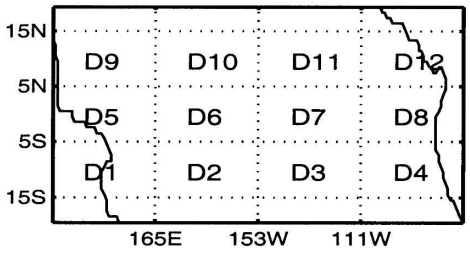

(b) ΔNino3_SSTA

0.056	0.046	0.044	0.014
0.046	0.098	0.193	0.061
0.013	0.026	0.038	0.009

(c) ΔW_{mix}

0.036	0.036	0.036	0.023
0.028	0.035	0.031	0.023
0.017	0.035	0.030	0.019

(d) η

1.571	1.257	1.236	0.609
1.641	2.774	6.120	2.658
0.776	0.724	1.238	0.446

FIG. 1. (a) The zones of local changes in DMC in expts D1–D12, (b) amplitude of SSTA in Niño-3 (°C), (c) amplitude of change in energy supporting mixing (TW), and (d) mixing efficiency for localized variability in the DMC (°C TW^{-1}).

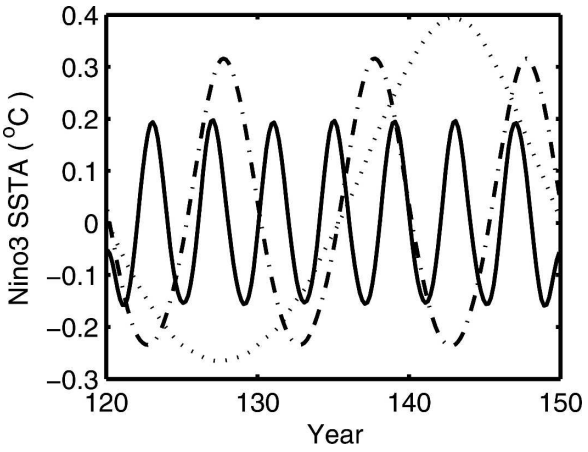

FIG. 2. Time evolution of SSTA in Niño-3 in expts B (solid line), C (dash–dot line), and D (dotted line).

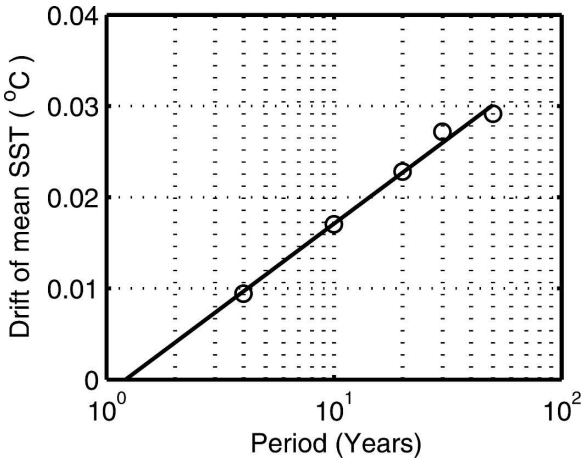

FIG. 3. Drift of $\overline{SST}$ in Niño-3 induced by oscillation in DMC of different periods.

(Fig. 3). The drift in $\overline{SST}$ at Niño-3 is closely associated with the nonlinearity of the circulation system as discussed below. Note that the drift in $\overline{SST}$ at Niño-3 indicates a change of the mean state of the equatorial circulation system, and such a drift can affect the time variability of the system; however, a systematic exploration of this dynamic issue is beyond the scope of this study.

In the second set of experiments, C, C1, C2, and C3, DMC was varied over the same period of 10 yr, but the amplitude of the variability in DMC was different (Table 1). Results from this set of experiments indicate that the range of SSTA, defined as ($SSTA_{max}$ − $SSTA_{min}$), in Niño-3 is approximately linearly proportional to the amplitude of the variability in DMC, $\Delta\kappa_d$ (Fig. 4).

Diagnosis of the model output indicates that the SSTA in Niño-3 is closely associated with great changes in the three-dimensional structure of the equatorial circulation system and the patterns of such changes seem independent of the period of the oscillation in DMC. Therefore, our analysis here is focused on experiment D with a period of 30 yr that is close to the first interdecadal time scale of Pacific decadal oscillation (Mantua and Hare 2002).

At the time of maximal DMC (year 128) SSTA is negative in the central-eastern equatorial Pacific and reaches a minimum in Niño-3, approximately −0.5°C (Fig. 5a). This local minimum in SSTA is due to the following mechanisms.

First, strong local diapycnal mixing entrains cold water from the subsurface layer and reduces the SST. The effect of varying mixing is expected to be stronger where there is a strong main thermocline close to the sea surface, and Niño-3 is exactly such a location.

Because of cooling in the upper ocean, the associated sea surface height anomaly (SSHA) is negative in the central-eastern equatorial Pacific (Fig. 5c). A negative SSHA in the central equatorial Pacific can reduce the westward surface pressure gradient force in the eastern basin and thus can enhance the westward surface flow (Fig. 5e). As a result, the reverse flow in the subsurface layer, the Equatorial Undercurrent, is also intensified, with an increase of volume flux of 3 Sv (1 Sv ≡ 10^6 m^3 s^{-1}) in the central equatorial Pacific (Fig. 6b). These changes are consistent with changes in vertical stratification along the equator. At the time of maximal DMC (year 128) the upper ocean, defined as water mass above the 20°C isotherm, is cooled down. Note that the depth of the 20°C isotherm at the western boundary remains basically unchanged (Fig. 7a). Thus, the slope

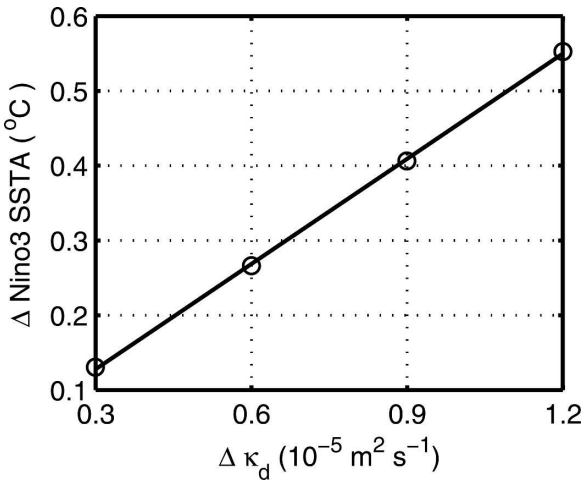

FIG. 4. The dependence of the range of SSTA in Niño-3 as a function of the amplitude of the variation in DMC.

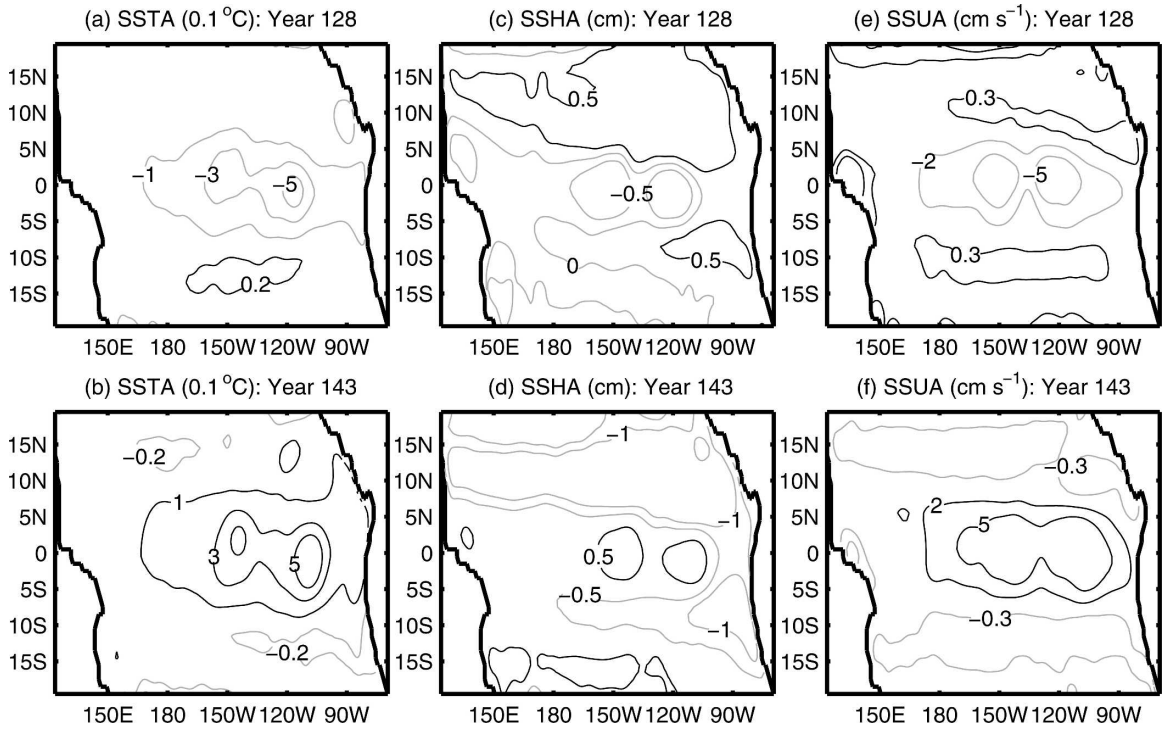

FIG. 5. (left) SSTA, (middle) SSHA, and (right) sea surface zonal current anomaly at the time of (top) maximal DMC and (bottom) minimal DMC taken from expt D.

of the equatorial main thermocline is enlarged, which is consistent with the stronger than normal Equatorial Undercurrent.

Second, SSTA at a given location, such as Niño-3, can be induced by changes in DMC in other locations. In fact, the anomaly of the Equatorial Undercurrent may be generated by a large-scale adjustment induced by DMC, which appears in the form of waves propagating through the ocean interior. Water with anomalous temperature transported by the Equatorial Undercurrent should also contribute to changes in SST. Note that at the time of maximal DMC, cooling is confined to the upper column only. In fact, when water in the surface layer is cooled, water in subsurface layers (below isotherm 20°C) is warmed up (Fig. 7a). Such a warming of the subsurface layer is partly due to the stronger than normal vertical mixing. In addition, this subsurface warming can also be attributed to the adjustment of the three-dimensional circulation system.

At the time of minimal DMC, the subsurface temperature anomaly flips its sign (Fig. 7b), and the corresponding changes in SSTA, SSHA, sea surface zonal current anomaly, and transport anomaly of the equatorial undercurrent also change their sign, as shown in Figs. 5b,d,f and 6b. Note that anomalies in this phase of DMC appear stronger than those in the phase of maximal DMC discussed above. In fact, in addition to the flipped signs along the equator, SSHA signals in the latitude band of 5°–15°N have signs opposite to the equatorial regime (Fig. 5). Similarly, SSTA in the extratropics have signs opposite to that in the equatorial regime. Thus, the oceanic response to spatially uniform

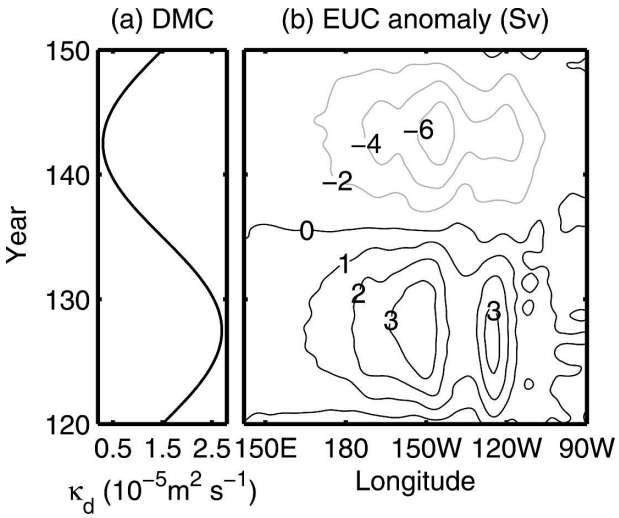

FIG. 6. (a) DMC and (b) time evolution of the volume transport anomaly of the Equatorial Undercurrent taken from expt D.

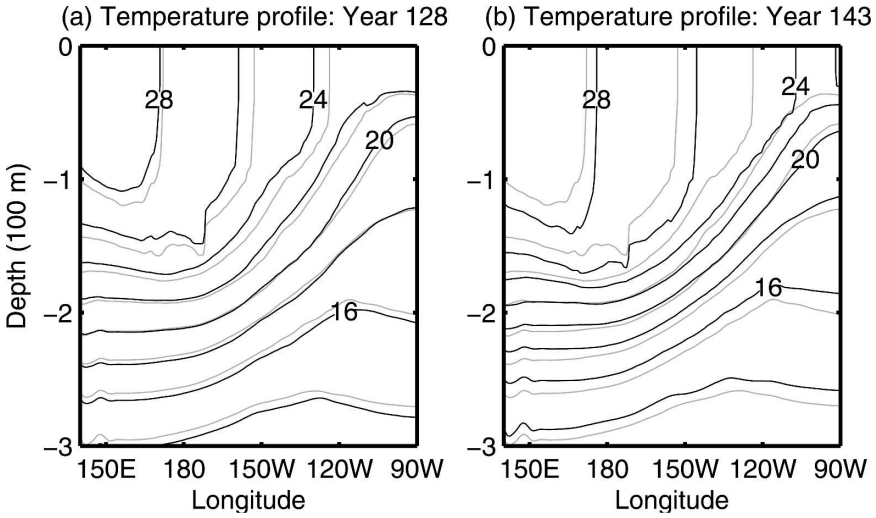

FIG. 7. Temperature profile along the equator for years (a) 128 and (b) 143 (gray curves for expt A and black curves for expt D; interval: 2°C).

changes in DMC is nonlinear and inhomogeneous in space, which is related to the three-dimensional nature of the equatorial circulation.

b. *Experiments with DMC varied over subdomains of the model basin*

The experiments discussed above are for the cases with DMC varied over the entire model basin uniformly. Another interesting question is whether localized time variability in the DMC can induce similar variability in the SST. In particular, the tropical cyclones tend to transfer a large amount of energy into a relatively small portion of the ocean. It is obvious that wind energy input from the tropical cyclones can definitely enhance the local diapycnal mixing rate greatly. However, the dynamic impact of the tropical cyclones may not be confined to the local circulation. Some studies have explored the dynamical effect of localized strong DMC on the meridional overturning rate. For example, based on numerical experiments on a simple boxlike model ocean mimicking the North Atlantic, Scott and Marotzke (2002) came to the conclusion that intensified DMC in place with strong stratification can enhance meridional overturning circulation more effectively. Boos et al. (2004) noticed that both the meridional overturning rate and poleward heat flux response to time-varying DMC in the oceanic interior react more sensitively than near the boundaries of the model basin.

This study is focused on the dynamical effect of time-varying DMC on SSTA in the equatorial ocean. To answer this question we carried out a third set of numerical experiments, series D1–D12, in which DMC was varied with an amplitude of $\Delta\kappa_d = 0.12 \times 10^{-4}$ m^2 s^{-1} with a period of 30 yr; however, periodic change in DMC was confined to some specific zones of the model basin only (Fig. 1a).

Similar to the cases discussed above, localized time-varying DMC can also induce periodic SSTA in the whole equatorial Pacific. Depending on the exact location of the localized time-varying DMC, spatial patterns of induced SSTA may vary; however, it is most interesting to compare SSTA appearing in Niño-3. The overall dynamical effect of time-varying DMC strongly depends on the location where DMC changes with time. For example, in experiment D9 the time-varying DMC is confined to a subregime in the northwest of the model basin. Volume transport of the Equatorial Undercurrent varied in a way similar to that of experiment D but with small amplitude of less than 1 Sv.

Two criteria are used to evaluate the dynamical effect of the localized changes in DMC. The first criterion is the amplitude of SSTA in Niño-3, ΔNino3_SSTA. The second criterion is the DMC efficiency defined as

$$\eta = \frac{\Delta\text{Nino3\_SSTA}}{\Delta W_{\text{mix}}}, \tag{2}$$

where ΔW_{mix} is the amplitude of change in energy supporting mixing, and mixing energy is diagnosed approximately from the model as

$$W_{\text{mix}} = \int\int \frac{g\kappa_d}{\alpha}(\rho_b - \rho_t)\, dx\, dy, \tag{3}$$

where $\alpha = 0.2$ is an empirical coefficient related to the efficiency of diapycnal mixing (Osborn 1980) and ρ_b and ρ_t are density on the sea floor and the uppermost layer below the buffer layer. Note that there is also

strong mixing in the mixed layer, and the maintenance of the dynamical structure of the mixed layer requires external mechanical energy, which comes primarily from wind stress input into the surface waves and Ekman layer (Wang and Huang 2004a,b). However, the focus of this study is on the energetics of the interior mixing; thus, the energetics balance of the mixed layer is beyond the scope of this paper and it is omitted in the following discussion.

It is readily seen that the most effective place to put the localized time-varying DMC is zone D7, which is roughly the same as Niño-3. In such a case, the amplitude of SSTA in Niño-3 is 0.19°C, much larger than that induced by time-varying DMC in other regions (Fig. 1b). The D6 zone is also an effective place to put in the perturbation in DMC; however, the corresponding amplitude of SSTA in Niño-3 is 0.1°C, about one-half of the value of zone D7. The least effective place to put the localized time-varying DMC is the southeast corner of the model basin. In addition, the localized time-varying DMC put in the northeast and southwest is not efficient.

The amplitude of change in energy required to support mixing is similar for most cases, and it is on the order of 0.03 TW (Fig. 1c). Note that energy required for D7 is 0.031 TW, so it is slightly smaller than some other runs. With a smaller amount of energy required to support the time-varying diapycnal mixing, experiment D7 is the most efficient run in terms of using external mechanical energy to produce the largest possible perturbation in SSTA in Niño-3 from the circulation system. In general, the equatorial band is the most effective place to apply the time-varying DMC, and the least effective place to apply the time-varying DMC is in the southeast, northeast, and southwest corners of the model basin (Fig. 1d).

For instances with the localized time-varying DMC applied to places outside of the Niño-3 zone, changes of SSTA in Niño-3 must be induced primarily by advection of the basin-wide circulation. Therefore, the equatorial zone is the most effective place to apply the time-varying DMC because the effects of change in the DMC can be carried to Niño-3 through the equatorial zonal currents. Experiment D7 is remarkable because a time-varying DMC can also directly affect the SSTA in Niño-3 through local vertical mixing and advection. However, for instances with a time-varying DMC placed on off-equator zones the effect of a time-varying DMC is remote and relatively ineffective.

Although Fig. 1d shows that mixing in the western Pacific is energetically less efficient in producing climate variability in the Tropics, note that our results are drawn under the assumption of the same amplitude of DMC. Changes of DMC may be spatially nonuniform in the ocean. In particular, changes of DMC in the regions with frequent activity of tropical cyclones may be much larger than that in other regions because of the great change in energy dissipation rate of tropical cyclones over the past decades (Emanuel 2005). Thus, tropical cyclones may have a large influence on the climate in the Tropics. Wind stress fields used in many previous studies are based on wind products, in which strong nonlinear events, such as hurricanes or typhoons, are smoothed out. As a result, the dynamic impacts of these nonlinear events cannot be truthfully reproduced in these studies.

c. Changes in the ocean interior induced by a time-varying DMC

It is now well known that large-scale oceanic waves, including both Kelvin waves and Rossby waves, play important roles in the adjustment of oceanic general circulation and ENSO in particular (McCreary 1983; Graham and White 1988). Early studies on the dynamical effect of the time-varying DMC have pointed out the role of Rossby waves. For example, Boos et al. (2004) noticed that time-varying DMC near the boundary can induce both boundary-trapped waves and westward-propagating Rossby waves, and a time-varying DMC in the oceanic interior can induce Rossby waves.

As external energy supporting diapycnal mixing varies, stratification in the ocean is altered in response, and these changes are intimately associated with global geostrophic adjustment processes in the form of large-scale waves, such as Rossby waves and Kelvin waves. Diagnosis of our numerical experiments indicates westward signal propagation in the subsurface layers. As an example, annual-mean depth anomaly of $\sigma_2 = 36$ is shown in Fig. 8. The mean depth of this isopycnal surface is approximately 600 m. The anomalies are formed near the eastern boundary and propagate westward. Near the eastern boundary the anomalous signals are roughly symmetric with respect to the equator; however, away from the eastern boundary they become asymmetric with larger amplitude in the Northern Hemisphere. On the other hand, anomalies in the Southern Hemisphere seem to penetrate deep into the subtropics. The asymmetric characters of anomalies reflect the asymmetric nature of forcing and the background stratification in the equatorial circulation.

The amplitude of anomalies and the westward propagation can be most readily seen near 10°N. During the peak DMC (year 128), depth anomaly is positive in the eastern basin, but it is negative in the western basin (Fig. 8b). Thus, the isopycnal surface in the eastern basin moves downward, but it moves upward in the

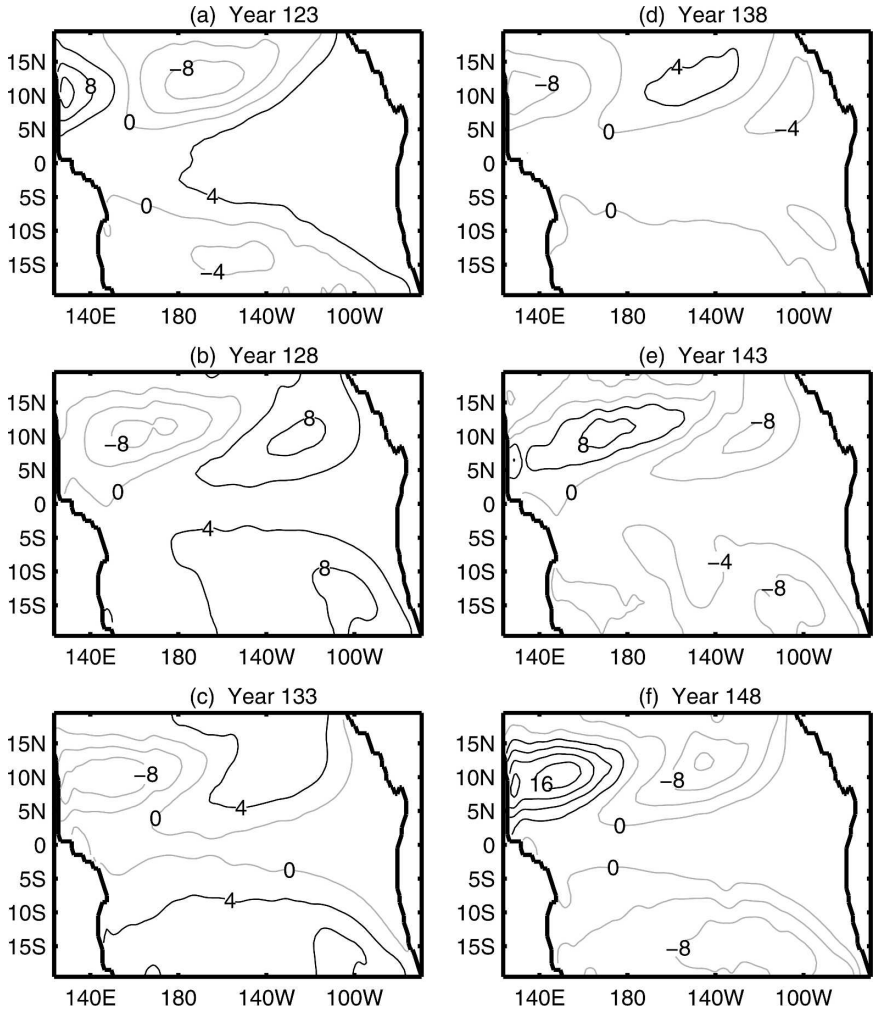

FIG. 8. Anomaly of the annual-mean depth of $\sigma_2 = 36.0$ in expt D for (a)–(f) years 123–148 (interval: 4 m).

western basin. On the other hand, depth of this isopycnal moves downward along the whole equatorial band, although the depth anomaly in the eastern equatorial ocean is slightly larger than in the western equatorial ocean. Note that on the annual-mean depth map there is no signal of wave propagation along the equator. This is because the equatorial Kelvin waves move so fast that the adjustment process associated with equatorial Kelvin waves can be considered as instantaneously finished; thus, they do not appear in such annual-mean maps.

Rossby waves can also be identified from the zonal section taken along a latitudinal circle off the equator (Fig. 9). It is readily seen that Rossby waves are produced near the eastern boundary and move westward. In experiment C on isopycnal $\sigma_2 = 36$, Rossby waves are produced right on the eastern boundary (Fig. 9a); however, on isopycnal $\sigma_2 = 36.6$, Rossby waves are produced at a location slightly west of the eastern boundary (Fig. 9b). The waves have a period of approximately 10 yr, and the signals generated near the eastern boundary take about 10 yr to reach the western boundary. Although amplitude of anomalies on $\sigma_2 = 36$ seems to decline slightly during the westward propagation, amplitude of these waves on both isopycnal surfaces remains basically unchanged over the whole basin. Note that the speed of these waves is slightly larger in the western basin, and this is probably due to the fact that the isopycnal surface in the western basin is deeper and the corresponding wave speed for the first baroclinic mode is enhanced (Chelton et al. 1998).

Depth anomalies on the same isopycnal surfaces for experiment D also appear in the form of Rossby waves (Figs. 9c,d). These waves take about 30 yr to propagate across the basin, which is longer than that in experiment C. These waves are induced by changes in DMC and

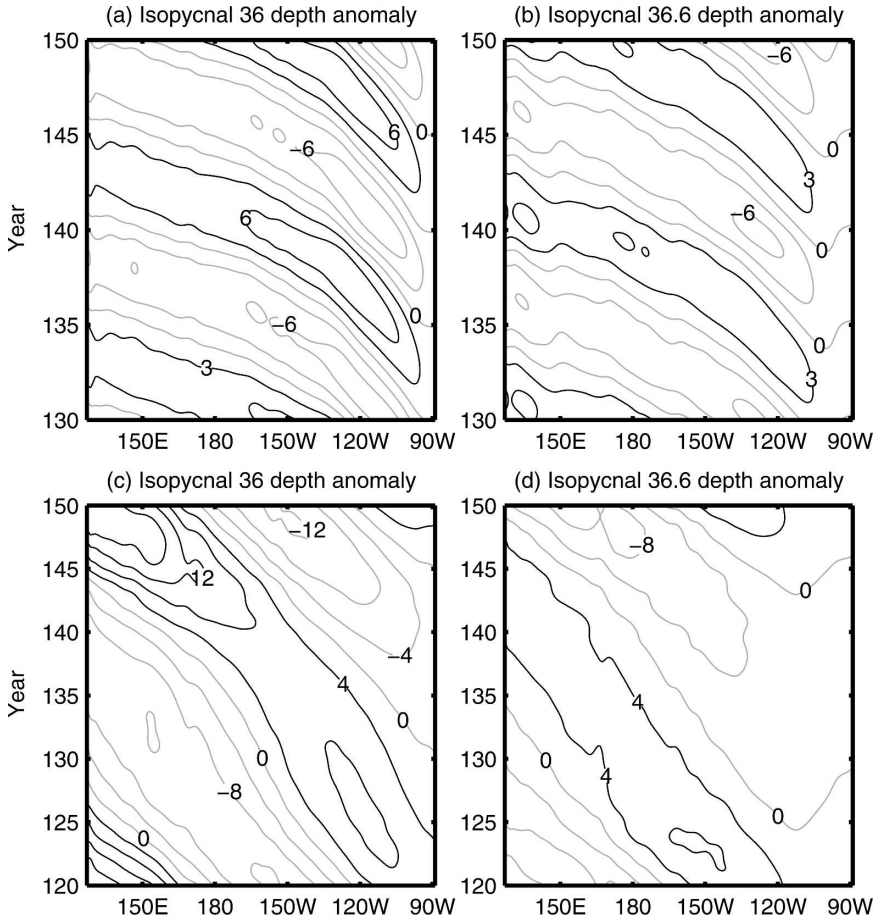

FIG. 9. Time-zonal plot of the depth anomaly for (left) $\sigma_2 = 36.0$ and (right) $\sigma_2 = 36.6$, taken from (top) expt C (interval: 3 m) and (bottom) expt D (interval: 4 m) along 11.5°N.

appear as a combination of different baroclinic modes. The changes in DMC with longer periods can produce higher-mode waves (Fig. 10); thus, the apparent wave signals will take longer time to propagate across the basin. Note that on the isopycnal surface $\sigma_2 = 36$ both the amplitude and the phase speed of the anomalies may increase during the westward movement. However, anomalies on the isopycnal surface $\sigma_2 = 36.6$ seem to behave differently.

The density anomaly has a complicated vertical structure, as shown in Fig. 10, where Figs. 10a,c are the depth anomaly in the isopycnal coordinate taken at the time of maximal DMC and Figs. 10b,d for the time of minimal DMC. In experiment C, at the time of maximum DMC the depth anomaly near the western boundary is positive, which implies all isopycnals deepen, while during the minimum DMC the depth anomaly near the western boundary is negative and does not change sign with depth; however, in the eastern basin depth anomaly appears in higher modes (Figs. 10a,b). For example, in year 143 it is positive in the upper and deep ocean, but it is negative at a middle depth.

In comparison, the vertical structure of the depth anomaly in experiment D is more complicated because of the existence of higher modes (Figs. 10c,d). The existence of higher modes is due to the fact that the forcing frequency is low enough exciting long-period baroclinic modes of Rossby waves in extratropics.

As these Rossby waves reach the western boundary, part of their energy is transformed into equatorward Kelvin waves that turn toward the equator where they continue to move eastward along the equatorial waveguide, thus inducing decadal variability in the equatorial ocean. Knutson and Manabe (1998) argued that decadal variability in the equatorial ocean might be induced by westward-propagating Rossby waves in extratropics. Figure 11 reveals an approximate annual-mean depth anomaly of the isopycnals under the mixed layer along the equator in experiment D at the time of the maximal DMC (year 128) and the minimal DMC (year

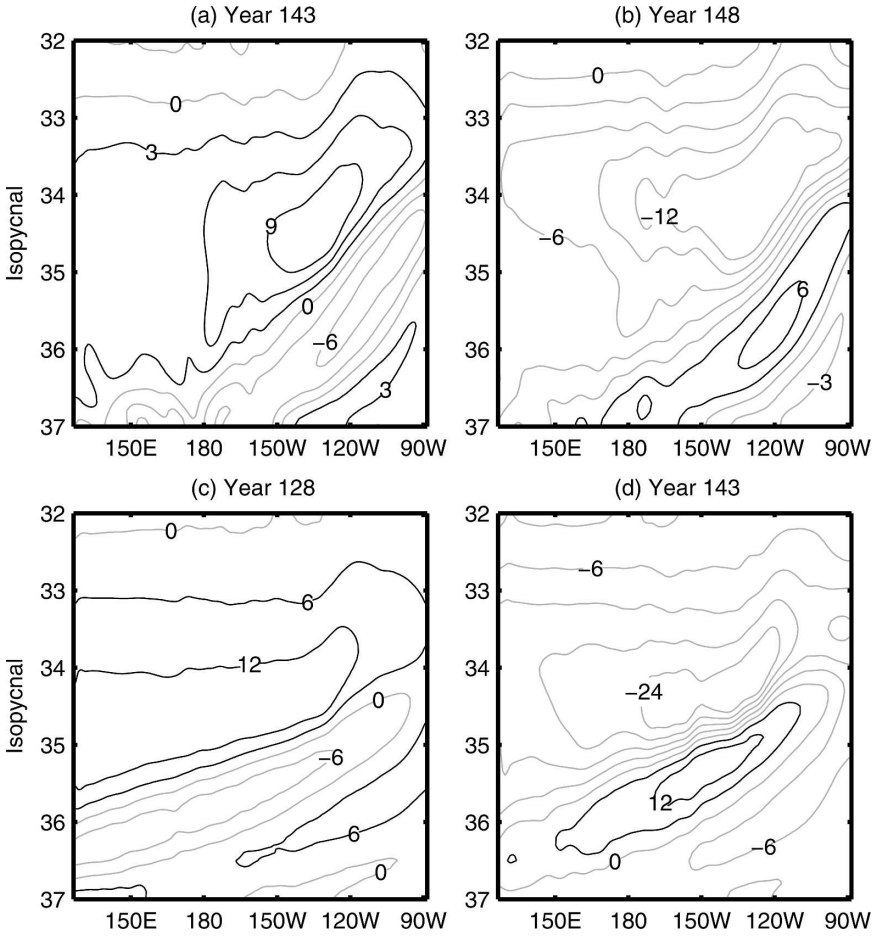

FIG. 10. Annual-mean depth anomaly of the isopycnals along 11.5°N in (top) expt C (interval: 3 m) for years (left) 143 and (right) 148 and in (bottom) expt D (interval: 6 m) for years (left) 128 and (right) 143.

143). The depth anomaly of isopycnal surfaces along the equator appears mainly in the form of the second baroclinic mode. At the time of DMC maximum, the depth anomaly is negative in the upper layer and positive in the lower layer (Fig. 11a). During the phase of DMC minimum, the depth anomaly reveals opposite signs (Fig. 11b). As discussed in previous publications (e.g., Huang and Pedlosky 1999; Liu 1999), anomalous cooling/heating at the upper ocean can induce climate variability in the subsurface ocean, which is primarily in the form of the second (or higher) baroclinic mode. Thus, our results are consistent with previous studies.

4. Combining dynamical effects caused by variation in DMC and wind stress

Some of the major factors not included in the experiments discussed above are changes in air–sea heat flux and the decadal variability in wind stress in the equatorial and subtropical Pacific. For example, changes in local wind stress can affect equatorial upwelling and thus change the local SST. In addition, change in local wind can affect SST through altering the air–sea heat flux and the zonal advection, as shown in recent studies (e.g., Wang and McPhaden 2000). Furthermore, changes in extratropical wind stress can influence the equatorial circulation remotely through the ocean bridge (Gu and Philander 1997; Huang and Wang 2001; McPhaden and Zhang 2002).

These factors have been explored extensively in the previous studies, most closely related to ENSO dynamics and decadal variability in the ocean. To isolate the contribution from small-scale mixing, we have purposely omitted the important effect of decadal changes in wind stress and heat flux. It is clear that a comprehensive understanding of long-term variability in the equatorial ocean can be gained through numerical experiments forced by the realistic combination of these factors.

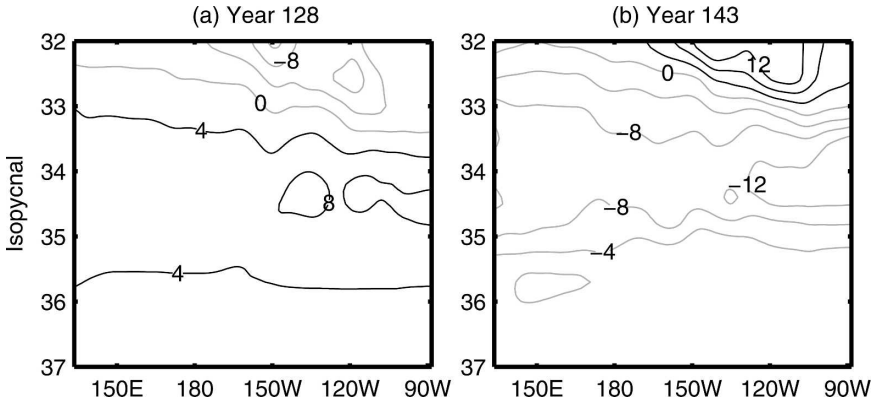

FIG. 11. Annual-mean depth anomaly of the isopycnals along the equator in expt D for years (a) 128 and (b) 143 (interval: 4 m).

Because of the preliminary statue of our knowledge of small-scale mixing parameterization, a satisfactory design of such numerical experiments remains a great challenge. Therefore, our aim in this section is to explore the possible outcome from such experiments through some simply designed experiments. In particular, we will be focused on the potential effect of decadal variability of wind stress in combination with variable DMC in the equatorial ocean.

Surface wind stress in the previous experiments is the monthly mean climatology. To examine the effect of DMC on the ocean with variable wind stress, two other experiments, W1 and W2, have been run, which were forced by decadal variable wind stress:

$$\boldsymbol{\tau} = \left(1 + 0.2 \sin \frac{2\pi t}{10}\right)\boldsymbol{\tau}_0, \tag{4}$$

where t is the time in units of year and $\boldsymbol{\tau}$ is the FSU monthly mean climatology of wind stress. The DMC is set to a constant in experiment W1. However, the DMC in experiment W2 is varied in the same way as in experiment C—that is, the maximal DMC occurs during the time of maximal wind forcing (Table 1).

The results show that decadal changes in wind stress in equatorial Pacific can be very efficient in causing large changes in SST. In fact, according to these experiments, 20% changes in wind stress or 80% changes in DMC can induce SSTA of the same magnitude (Fig. 12), although 80% variability in DMC may seem too large and unrealistic as compared with 20% change in wind stress. Taking results from these experiments, one may come to the conclusion that wind stress changes are more efficient in driving changes in SST than are changes in DMC. However, the dynamical contributions from wind stress and DMC are nearly superpositioned, as shown by the dotted line in Fig. 12.

There are two important points related to this issue. First, even if variability in DMC is less effective than that in wind stress changes, decadal variability in DMC may still be a nonnegligible contribution to the decadal variability of the equatorial circulation. Second, we have no reliable data or theory to quantify the variability of DMC on decadal time scale. In particular, recent work by Emanuel and his colleagues suggested that there is a chance that mechanical energy supporting diapycnal mixing in the equatorial ocean may vary greatly because of the contribution from nonlinear events like the tropical hurricanes or typhoons (Bister and Emanuel 2002; Emanuel 2005). Because of the tremendous difference between the spatial and temporal scales of turbulence and internal waves in the ocean and the resolutions that are affordable in the currently used oceanic general circulation models, there remains a grand challenge in parameterizing such nonlinear

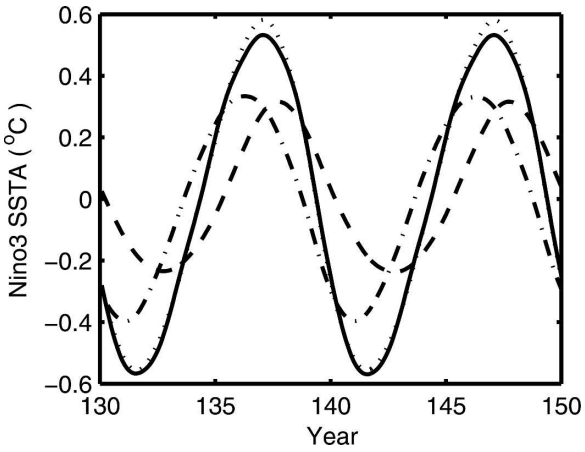

FIG. 12. Time evolution of SSTA in Niño-3 in expts C (dashed line), W1 (dash–dot line), W2 (solid line), and the superposition of SSTA in Niño-3 in expts C and W1 (dotted line).

physics into oceanic general circulation models. Therefore, realistic simulation of equatorial circulation, including realistic combination of decadal variability in wind stress, heat flux, and DMC, will be an exciting research frontier in future studies.

5. Conclusions

We have carried out numerical experiments to test the ideas that decadal variability in DMC may induce noticeable anomalies in the equatorial Pacific Ocean. As DMC oscillates periodically, the whole equatorial circulation is forced into a periodic cycle. Such a periodic cycle is intimately associated with changes in the equatorial current system and SST. In particular, at the time of maximal DMC, SST in the central equatorial Pacific is cooled down by a stronger-than-normal diapycnal mixing, and the effect of stronger mixing works most efficiently over the area of a strong near-surface main thermocline, that is, a place like Niño-3. Surface cooling leads to a decline of sea surface height in the central Pacific. In addition, it can also induce a negative anomaly in the west–east pressure force in the surface layer. The decline in the zonal pressure force enhances the westward flow in the surface layer and the eastward flow associated with the Equatorial Undercurrent.

Experimental results on the localized time-varying DMC are very interesting. Regardless of the location of the localized time-varying DMC, the notable amplitude of SSTA always appears in Niño-3. It is not surprising that the most efficient location of applying time-varying DMC is Niño-3 and its vicinity, that is, both the amplitude of SSTA and the efficiency of the perturbations, as defined above, are the highest if the time-varying DMC is put in Niño-3 or its vicinity. In addition, the equatorial currents, including the surface currents and the Equatorial Undercurrent, work together to produce SSTA. On the other hand, if time-varying DMC is far away from Niño-3, its dynamical influence is remote and less efficient because it has to go through the current system.

The most important result from our numerical experiments is that time-varying DMC may be a nonnegligible contributor to the decadal variability of the nonlinear air–sea interaction in the equatorial Pacific. For idealized cases discussed in this study, a model ocean under climatological mean wind stress and thermohaline forcing can develop decadal variability in SSTA, with amplitude on the order of 0.5°C in Niño-3, which is very strong and is comparable to the amplitude of decadal variability observed.

From an energetics point of view, wind energy over the global ocean calculated from the daily mean wind stress showed that the mechanical energy input to the ocean increased more than 20% over the past 30 yr (Wang and Huang 2004a,b; Huang et al. 2006), and, most important, energy dissipation rate of tropical cyclones almost doubled during the same time period (Emanuel 2005). Since the mechanical energy input to the ocean can be transferred to a great distance via internal waves, it is speculated that the amplitude of time-varying DMC in the equatorial Pacific Ocean will have large amplitude. The next step in this line of research is to implement the time-varying DMC in a commonly accepted ENSO model to see how the model's decadal variability would be altered. A vital component of such numerical experiments associated with the specification of the time-varying DMC remains somewhat subjective and thus needs to be improved as new theory and parameterization come along.

Of course, the exact pathway for the mechanical energy from wind stress to internal wave breaking in the ocean interior remains unclear at this time. Thus, further study of the energetics of the oceanic circulation and its impact on large-scale climate problem is needed.

Acknowledgments. CJH and WW were supported by The National Natural Science Foundation of China through Grant 40476010 and National Basic Research Priorities Programmer of China through Grant 2005CB422302. RXH was supported by the National Oceanic and Atmospheric Administration through CICOR Cooperative Agreement NA17RJ1223 to the Woods Hole Oceanographic Institution. This study is also supported through the Chinese 111 Project under Contract B07036. Comments by the two anonymous reviewers helped to improve this manuscript greatly.

REFERENCES

Alford, M. H., 2003a: Improved global maps and 54-year history of wind-work on ocean inertial motions. *Geophys. Res. Lett.,* **30,** 1424, doi:10.1029/2002GL016614.

——, 2003b: Redistribution of energy available for ocean mixing by long-range propagation of internal waves. *Nature,* **423,** 159–162.

Bister, M., and K. A. Emanuel, 2002: Low frequency variability of tropical cyclone potential intensity. I: Interannual to interdecadal variability. *J. Geophys. Res.,* **107,** 4801, doi:10.1029/2001JD000776.

Boos, W. R., J. R. Scott, and K. A. Emanuel, 2004: Transient diapycnal mixing and the meridional overturning circulation. *J. Phys. Oceanogr.,* **34,** 334–341.

Chelton, D. B., R. A. deSzoeke, M. G. Schlax, K. El Naggar, and N. Siwertz, 1998: Geographical variability of the first baroclinic Rossby radius of deformation. *J. Phys. Oceanogr.,* **28,** 433–460.

Emanuel, K. A., 2001: Contribution of tropical cyclones to meridional heat transport by the oceans. *J. Geophys. Res.,* **106,** 14 771–14 781.

——, 2005: Increasing destructiveness of tropical cyclones over the past 30 years. *Nature,* **436,** 686–688.

Garrett, C., and L. St. Laurent, 2002: Aspects of deep ocean mixing. *J. Oceanogr.,* **58,** 11–24.

Gates, W. L., and A. B. Nelson, 1975: A new (revised) tabulation of the Scripps topography on a one-degree grid. Part 1: Terrain heights. Tech. Rep. R-1276-1-ARPA, The Rand Corporation, 132 pp.

Gent, P. R., and J. C. McWilliams, 1990: Isopycnal mixing in ocean circulation models. *J. Phys. Oceanogr.,* **20,** 150–155.

Graham, N. E., and W. B. White, 1988: The El Niño cycle: A natural oscillator of the Pacific ocean–atmosphere system. *Science,* **240,** 1293–1302.

Griffies, S. M., and R. W. Hallberg, 2000: Biharmonic friction with a Smagorinsky-like viscosity for use in large-scale eddy-permitting ocean models. *Mon. Wea. Rev.,* **128,** 2935–2946.

——, and Coauthors, 2000: Developments in ocean climate modelling. *Ocean Modell.,* **2,** 123–192.

Gu, D., and S. G. Philander, 1997: Interdecadal climate fluctuations that depend on exchanges between the Tropics and extratropics. *Science,* **275,** 805–807.

Hallberg, R., 1997: Stable split time stepping schemes for large-scale ocean modeling. *J. Comput. Phys.,* **135,** 54–65.

——, 2000: Time integration of diapycnal diffusion and Richardson number–dependent mixing in isopycnal coordinate ocean models. *Mon. Wea. Rev.,* **128,** 1402–1419.

——, and P. Rhines, 1996: Buoyancy-driven circulation in an ocean basin with isopycnals intersecting the sloping boundary. *J. Phys. Oceanogr.,* **26,** 913–940.

Huang, R. X., 1999: Mixing and energetics of the oceanic thermohaline circulation. *J. Phys. Oceanogr.,* **29,** 727–746.

——, 2004: Ocean, energy flows in. *Encyclopedia of Energy,* C. J. Cleveland, Ed., Vol. 4, Elsevier, 497–509.

——, and J. Pedlosky, 1999: Climate variability inferred from a layered model of the ventilated thermocline. *J. Phys. Oceanogr.,* **29,** 779–790.

——, and Q. Wang, 2001: Interior communication from the subtropical to the tropical oceans. *J. Phys. Oceanogr.,* **31,** 3538–3550.

——, W. Wang, and L. L. Liu, 2006: Decadal variability of wind energy input to the World Ocean. *Deep-Sea Res. II,* **53,** 31–41.

Knutson, T. R., and S. Manabe, 1998: Model assessment of decadal variability and trends in the tropical Pacific Ocean. *J. Climate,* **11,** 2273–2296.

Kraus, E. B., and J. S. Turner, 1967: A one-dimensional model of the seasonal thermocline. II: The general theory and its consequences. *Tellus,* **19,** 98–106.

Large, W. G., J. C. McWilliams, and S. C. Doney, 1994: Oceanic vertical mixing: A review and a model with a nonlocal boundary layer parameterization. *Rev. Geophys.,* **32,** 363–403.

Legler, D. M., and J. J. O'Brien, 1988: Tropical Pacific wind stress analysis for TOGA. *IOC Series of Ocean Measurements,* ICO Technical Series 33, Vol. 4, UNESCO, 11–17.

Levitus, S., and T. P. Boyer, 1994: *Temperature.* Vol. 4, *World Ocean Atlas 1994,* NOAA Atlas NESDIS 4, 117 pp.

——, R. Burgett, and T. P. Boyer, 1994: *Salinity.* Vol. 3, *World Ocean Atlas 1994,* NOAA Atlas NESDIS 3, 99 pp.

Liu, Z., 1999: Forced planetary wave response in a thermocline gyre. *J. Phys. Oceanogr.,* **29,** 1036–1055.

Loder, J. W., and C. Garrett, 1978: The 18.6-year cycle of sea surface temperature in shallow seas due to variations in tidal mixing. *J. Geophys. Res.,* **83** (C4), 1967–1970.

Mantua, N. J., and S. R. Hare, 2002: The Pacific decadal oscillation. *J. Oceanogr.,* **58,** 35–44.

——, ——, Y. Zhang, J. M. Wallace, and R. C. Francis, 1997: A Pacific interdecadal climate oscillation with impacts on salmon production. *Bull. Amer. Meteor. Soc.,* **78,** 1069–1079.

McCreary, J. P., 1983: A model of tropical ocean–atmosphere interaction. *Mon. Wea. Rev.,* **111,** 370–387.

McDermott, D. A., 1996: The regulation of northern overturning by Southern Hemisphere winds. *J. Phys. Oceanogr.,* **26,** 1234–1255.

McPhaden, M. J., and D. Zhang, 2002: Slowdown of the meridional overturning circulation in the upper Pacific Ocean. *Nature,* **415,** 603–608.

Mellor, G. L., and T. Yamada, 1982: Development of a turbulence closure model for geophysical fluid problems. *Rev. Geophys.,* **20,** 851–875.

Munk, W., and C. Wunsch, 1998: Abyssal recipes II: Energetics of tidal and wind mixing. *Deep-Sea Res.,* **45,** 1977–2010.

Nagasawa, M., Y. Niwa, and T. Hibiya, 2000: Spatial and temporal distribution of the wind-induced internal wave energy available for deep water mixing in the North Pacific. *J. Geophys. Res.,* **105** (C6), 13 933–13 943.

Osborn, T. R., 1980: Estimates of the local rate of vertical diffusion from dissipation measurements. *J. Phys. Oceanogr.,* **10,** 83–89.

Pacanowski, R. C., and S. G. H. Philander, 1981: Parameterization of vertical mixing in numerical models of tropical oceans. *J. Phys. Oceanogr.,* **11,** 1443–1451.

Sandström, J. W., 1908: Dynamische Versuche mit Meerwasser. *Ann. Hydrogr. Marit. Meteor.,* **36,** 6–23.

——, 1916: Meteorologische studien im schwedischen Hochgebirge. *Goteborgs K. Vetensk. Vitterhets-Samh Handl.,* Ser. 4, Vol. 22, No. 2, 48 pp.

Scott, J. R., and J. Marotzke, 2002: The location of diapycnal mixing and the meridional overturning circulation. *J. Phys. Oceanogr.,* **32,** 3578–3595.

Smagorinsky, J., 1963: General circulation experiments with the primitive equations. Part I: The basic experiment. *Mon. Wea. Rev.,* **91,** 99–164.

Thompson, L., K. A. Kelly, D. Darr, and R. Hallberg, 2002: Buoyancy and mixed layer effects on the sea surface height response in an isopycnal model of the North Pacific. *J. Phys. Oceanogr.,* **32,** 3657–3670.

Wang, W., and M. J. McPhaden, 2000: The surface-layer heat balance in the equatorial Pacific Ocean. Part II: Interannual variability. *J. Phys. Oceanogr.,* **30,** 2989–3008.

Wang, W., and R. X. Huang, 2004a: Wind energy input to the Ekman layer. *J. Phys. Oceanogr.,* **34,** 1267–1275.

——, and ——, 2004b: Wind energy input to the surface waves. *J. Phys. Oceanogr.,* **34,** 1276–1280.

——, and ——, 2005: An experimental study on thermal circulation driven by horizontal differential heating. *J. Fluid Mech.,* **540,** 49–73.

Wright, D. G., 1997: An equation of state for use in ocean models: Eckart's formula revisited. *J. Atmos. Oceanic Technol.,* **14,** 735–740.

Wunsch, C., 1998: The work done by the wind on the ocean general circulation. *J. Phys. Oceanogr.,* **28,** 2332–2340.

——, and R. Ferrari, 2004: Vertical mixing, energy and the general circulation of the oceans. *Annu. Rev. Fluid Mech.,* **36,** 281–314.

Zhai, X., R. J. Greatbatch, and J. Sheng, 2004: Advective spreading of storm-induced inertial oscillations in a model of the northwest Atlantic Ocean. *Geophys. Res. Lett.,* **31,** L14315, doi:10.1029/2004GL020084.